Surfactant-assisted cerium oxide and its catalytic activity towards Fenton process for non-degradable dye

Bhawana Jain[1] · Ajaya K. Singh[1] · Ayesha Hashmi[1] · Md. Abu Bin Hasan Susan[2] · Jean-Paul Lellouche[3]

Abstract

Water pollution kills nearly 2 million people and costs trillions of dollars every year, which continuously threatens the survival of both human and animal species in the world. The textile industry is considered as pollutant-releasing industries in water. In this research work, we firstly report the synthesis of cerium oxide (CeO_2) nanoparticles in the range of quantum dots (QDs). Syntheses of cerium oxide nanomaterials were assisted by using three different surfactants, i.e., sodium dodecyl sulfate (SDS; anionic), cetyltrimethylammonium bromide (CTAB; cationic), and cetylpyridinium chloride (CPC; cationic); the surfactants control the growth and particle size of the prepared material. The nanomaterials were characterized by UV-visible spectroscopy, X-ray diffractometer (XRD), scanning electron microscopy (SEM), energy-dispersive X-ray (EDX) analysis, high-resolution transmission electron microscopy (HRTEM), and thermogravimetric/differential thermal analyses (TG/DTA), together with Fourier transform infrared (FTIR) spectroscopy and photoluminescence (PL). The particle size of such CeO_2 nanoparticles ranges between 1.66 and 4.36 nm. Their catalytic role was successfully investigated in Fenton reaction for the oxidative removal of methylene blue (MB) dye. The efficiency of Fenton reaction using such CeO_2 QDs has been used to highlight the importance of such nanosized catalysts for wastewater treatment.

1 Introduction

Nowadays, different technologies have emerged and focused on the use of quantum dots (QDs) in the development and progress of all areas of life, which include social, industrial, and economic fields. The quantum dots are generally fabricated to synthesize and design a nanoscale system for improvements in biomedical, sensing, and bioimaging performances [1, 2]. Cerium oxide (CeO_2) is a fluorite type of rare earth oxide. It finds applications as intense insulators, high refractive index materials, gas sensors, polishing materials, sunscreens, oxygen storage, and antibacterial agents and plays an important role in industry activities [3–5]. Cerium oxide is also known to be a marvelous catalyst with a low cost that provides high surface area for any catalytic reaction [6–8]. Over the past two decades, CeO_2 nanoparticles (NPs) have been widely used in nano-medicine, fuel cell, and catalysis [9–11]. Moreover, the cytotoxic effect of CeO_2 NPs has been studied with *Escherichia* coli and human lung cancer cells [12, 13]. In this context, there are various nanofabrication methods such as chemical vapor deposition, sonochemical preparation, sol-gel process, ball milling, photo-induced conversion, biological synthesis, and chemical precipitation methods used for CeO_2 preparation. In contrast to other fabrication techniques, chemical precipitation method has been widely adopted for nanofabrication due to its simplicity, versatility, and cost-effective route. This process offers low temperatures for nanoparticle growth and less time and thus, the chemical precipitation is one of the most exclusive techniques for CeO_2 synthesis.

The nanofabrication of nanoparticles using appropriate surfactant enhances their catalytic surface area and reduces the agglomeration of resulting particles [14]. Various surfactants have so far been used for the nanofabrication of CeO_2 NPs,

✉ Ajaya K. Singh
ajayaksingh_au@yahoo.co.in

1 Department of Chemistry, Govt. V. Y. T. PG. Autonomous College, Durg, Chhattisgarh 491001, India

2 Department of Chemistry, University of Dhaka, Dhaka, Bangladesh

3 Department of Chemistry & Institute of Nanotechnology & Advanced Materials (BINA), Bar-Ilan University, Ramat Gan, Israel

including cationic [15–17], non-ionic [18, 19], and anionic [20, 21] surfactants. It was assumed that the cationic surfactant can easily adsorb onto the surface of generated CeO_2 due to the high electronegativity of oxygen atoms. CeO_2 NPs accumulate in water, after their use in water treatment. However, there is little non-significant information about their toxicological effects on human and aquatic life [22]. In the present research work, CeO_2 QDs were successfully prepared. The sizes of the resulting nanoparticles have been compared with previously reported data [23–31].

Water contains various pollutants [32]. Among these pollutants, organic dyes are frequently used and continuously disposed of for several purposes such as dyeing clothes, leather, and furniture, even in our regular life in food, cosmetics, and medicine. Dyes are non-biodegradable and have long-term effects on exhibiting hazard effects on aquatic environment [33]. In 2017, a detergent-making industry disposed of blue dye into Kasadi River, Taloja (India) without any treatment and its residual dye powder into the air, which created harm to the environment. The Maharashtra Pollution Control Board has been warned of a shutdown. So, it is necessary to use any sophisticated and reliable method to break the bigger molecule of dyes into many smaller fragments, such as water, carbon dioxide, and some other byproducts. Dyes can be degraded by various methods, e.g., biomass degradation [34], catalytic degradation [35], combined treatment [36], Fenton and Fenton-like processes [37], and heterogeneous photocatalysis [38]. Among these, the Fenton process is the best-advanced oxidation process (AOP) and is based on the generation of a powerful oxidizing agent such as hydroxyl radicals ($^\bullet OH$) at significant concentrations to effectively decontaminate water [39]. Many different kinds of AOPs have been developed to produce in situ $^\bullet OH$ radicals [40].

Methylene blue (MB, $C_{16}H_{18}ClN_3S$) is a cationic thiazine dye that is highly used as an indicator [41] in iodometric titration. It is most frequently used in the medical field and suggested that its high use affects the nervous system [42]. The World Health Organization (WHO) listed it as an essential medicine with the most effective and safe medicine factor. Oxidation and adsorption of MB by various Fenton-like reactions and the catalytic process was earlier reported using different catalysts, such as Fe^{2+}, titanomagnetite, ferrocene, Fe_3O_4-GO-TiO_2, ultraviolet/vacuum ultraviolet, $Fe_{3-x}Ti_xO_4$, chitosan cross-linked ferrous complex, reduced graphene oxide-Fe_3O_4 nanocomposites, iron-amended activated carbon, and magnetic nanocomposites [43–48]. In the present work, we used CeO_2 as a catalyst in Fenton process and compared it with other catalysts. Major advantages of using

CeO_2 are as follows: this catalyst effectively works on pH 5–7; it does not need any additional process to remove MB and thus is cost-effective and simple; it is highly stable when used in five consecutive cycles for MB degradation; and finally, its quantum size makes it useful for other purposes, i.e., sensor, fuel cell, medicine, etc.

Here, we report for the first time the synthesis of CeO_2 NPs by using a surfactant-mediated precipitation methodology in which the particle size and morphology are ultimately confined into a quantum dots range towards its application as a heterogeneous catalyst in any Fenton reaction for removal of thiazine dye.

2 Experimental details

2.1 Materials

AR grade reagents were used throughout the reaction. Cerium sulfate (S. D. Fine, India) was used as a cerium precursor. An anionic surfactant, sodium dodecyl sulfate (SDS), and two cationic surfactants, cetyltrimethylammonium bromide (CTAB) and cetylpyridinium chloride (CPC), were purchased from Sigma Aldrich. $NH_3.H_2O$ was added to maintain the pH of the reaction medium for CeO_2 synthesis. MB dye was obtained from S. D. Fine Chemicals and used without further purification. Sodium hydroxide (1 M), sulfuric acid (1 M), and hydrogen peroxide (30% w/w) from Merck were used.

2.2 Synthesis of CeO₂ QDs

CeO_2 quantum dots have been prepared by a simple precipitation method using different cationic and anionic surfactants in the aqueous solution. First, the homogeneous solution of 0.1 M CTAB/CPC/SDS (surfactant) was prepared, and then 10 mL of ammonia solution (25%) was added with continuous stirring. 0.1 M cerium sulfate phase was mixed with the surfactant solution under vigorous stirring for 2 h. The obtained CeO_2-based product was kept for 30-min-long aging. Prepared particles were washed thoroughly many times with double-distilled water (ddH_2O) to remove excess surfactant.

2.3 Characterization of CeO₂ QDs

UV-visible absorption spectra were obtained by Cary 5000. The XRD patterns were recorded to characterize the crystallinity and phase purity of QDs by Bruker D-8 Advance X-ray diffractometer with CuK$\propto$ X-ray radiation with $\lambda = 0.15496$ nm operated at 40 kV and 40 mA in the 2 range of 10–80°. SEM analyses were performed by using JEOL-JSM 6390, which helped to find/analyze the surface morphology of the QDs. TEM measurements were carried out on a
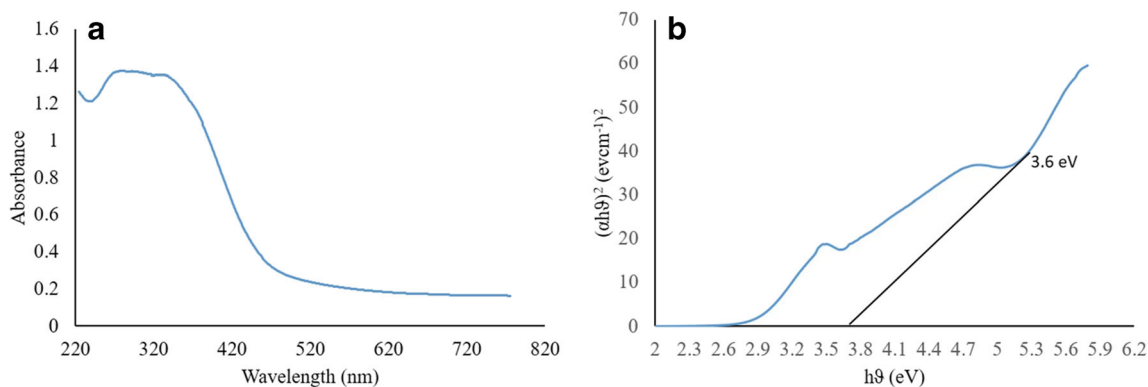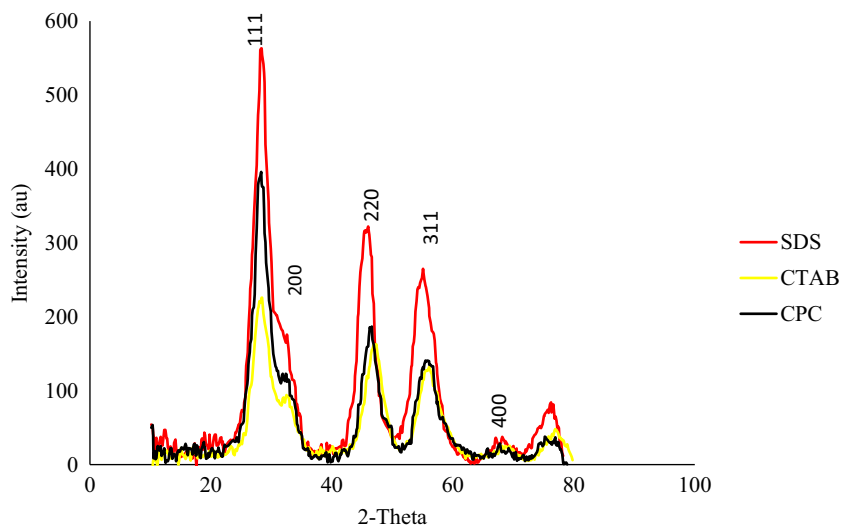
Fig. 1 a Optical absorption spectrum of CeO$_2$ QDs with UV-visible spectroscopy. b Plot of $(\alpha h\vartheta)^2$ versus hϑ for synthesized CeO$_2$ QDs

Zeiss EM 912 Ω instrument at an acceleration voltage of 120 kV, which confirmed the synthesis of QDS by particle size determination. TGA analyses were carried out by using a Perkin Elmer Diamond instrument with a heating rate of 20 °C/min. FTIR spectra were taken by FTIR 8400S, Shimadzu, while photoluminescence analyses were taken by JY Fluorog-3-11 with xenon lamp 450 W in a 180–850-nm range.

2.4 Kinetic study

MB was selected as a model pollutant because of its ease of monitoring by discoloration of the dye. Degradation of MB by heterogeneous Fenton reaction was carried out in a UV-visible spectrophotometer (Cary win UV Bio 50) by monitoring absorbance. A detailed parametric study was carried out successfully. A CeO$_2$QD was used as a catalyst for the degradation of MB (15 mg/L) at pH 6 under sunlight. Initially, MB concentration was determined through its absorbance at 665 nm. Then, the reaction was commenced by adding H$_2$O$_2$ to the reaction mixture, which contains all other reactants (MB, CeO$_2$) with continuous stirring at 400 rpm after 30 min of dark adsorption.

3 Results and discussion

3.1 Characterization studies

UV-visible absorption spectra reveal the electronic structure of the obtained CeO$_2$. It is related to band gap energy. The UV-visible absorption data provide a reliable estimate of the bandgap. Prepared CeO$_2$ QDs showed a broad peak between 280 and 330 nm with an absorbance of 1.37 (Fig. 1a).

Band gap energy can be calculated by a plot between $(\alpha h\vartheta)^2$ versus photon energy, hϑ (Fig 1b), where α is the absorbance calculated from UV [49]. hϑ is calculated from wavelength using

$$h\vartheta = 1240/\text{wavelength} \qquad (1)$$

Extrapolating the straight-line portion of the curves to zero absorption coefficient value gives the value of band gap energy. Optical studies also show a blue shift at 3.6 eV with respect to bulk material at 3.15 eV due to quantum-confined exciton absorption; this confirms the synthesis of CeO$_2$ QDs.

Fig. 2 XRD patterns of the as-synthesized CeO$_2$ QDs by using different surfactants

Table 1 Value of different parameters obtained by Eqs. 2–6

CeO$_2$ by different surfactant	d (interlayer spacing)		Average crystallite size (D) (nm) (by Debye-Scherrer)	δ (dislocation density) × 10^{-14} lines/m^2	ε strain × 10^{-3}
	By Bragg's equation	By TEM images			
SDS	0.32	0.35	2.1	2400	0.012622
CTAB	0.31	0.28	2.2	2260	0.012850
CPC	0.31	0.30	2.4	1816	0.069000

It was already known that not a single crystal is perfect due to its finite size. Thus, this imperfection is a reason behind the observed broadening of the diffraction peak of the crystal. Through the peak width analysis, we can determine crystallite size and lattice strain. X-ray peak profile analysis has been used to determine the microstructural quantities and correlate them to the observed material properties [50].

XRD patterns of CTAB, SDS, and CPC-assisted synthesized CeO$_2$ QDs are shown in Fig. 2. The XRD peaks of corresponding planes (111, 200, 220, 311, 400) are located at 28.08°, 33.02°, 46.99°, 55.94°, and 69.34° respectively, revealing the synthesis of a face-centered cubic fluorite structure of CeO$_2$ in agreement with those of bulk CeO$_2$. Diffraction from a crystal has been calculated by using Bragg's equation (2):

$$2d \, \mathrm{Sin}\theta = n\lambda \tag{2}$$

In this equation, n is the order of diffraction (usually $n = 1$), λ is the wavelength of CuKα radiation (0.15406 nm); d is the spacing between planes of given Miller indices h, k, and l. In CeO$_2$ face-centered cubic structured spacing of the plane, the lattice constant and Miller indices are related as follows:

$$d_{hkl} = \frac{a}{\sqrt{h^2 + k^2 + l^2}} \tag{3}$$

Thus, the average crystallite size can be calculated with the help of Debye-Scherrer's equation below.

$$D = 0.89\lambda / \beta cos\theta \tag{4}$$

where β = line broadening in radians, θ = Bragg's angle of the peak, and λ = X-ray wavelength.

The full width at half maxima (FWHM) of the XRD peaks might also contain a contribution from the lattice strain. The average strains of the CeO$_2$ QDs were calculated by using Stokes-Wilson equation:

$$\varepsilon_{str} = \beta / 4tan\theta \tag{5}$$

The dislocation density (δ) has been evaluated from relating Williamson-Smallman's formulae.

$$\delta = 1/D^2 \, \mathrm{lines/m}^2 \tag{6}$$

With the help of XRD data, i.e., FWHM and theta value, and by Eqs. 2–6, different basic parameters of a crystal have been calculated (Table 1).

Figure 2 shows an intensely sharp and narrow peak for CeO$_2$ synthesized by anionic surfactant while cationic surfactants, i.e., CTAB and CPC peaks are broad. Their intensities are reduced, i.e., the order of peak intensities via the use of different surfactants is SDS > CPC > CTAB. Similarly, peak broadening is also decreased in the same manner. Smallest crystal size has also been obtained with SDS-mediated CeO$_2$ QDs. Morphologies of CeO$_2$ QDs are shown using SEM images in Fig. 3a–c. CeO$_2$ QDs show an irregular morphology

Fig. 3 SEM images of synthesized CeO$_2$ QDs via **a** SDS, **b** CTAB, and **c** CPC
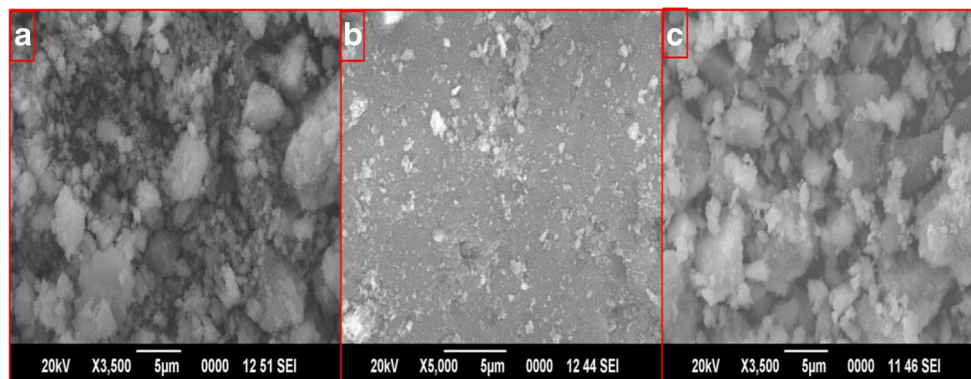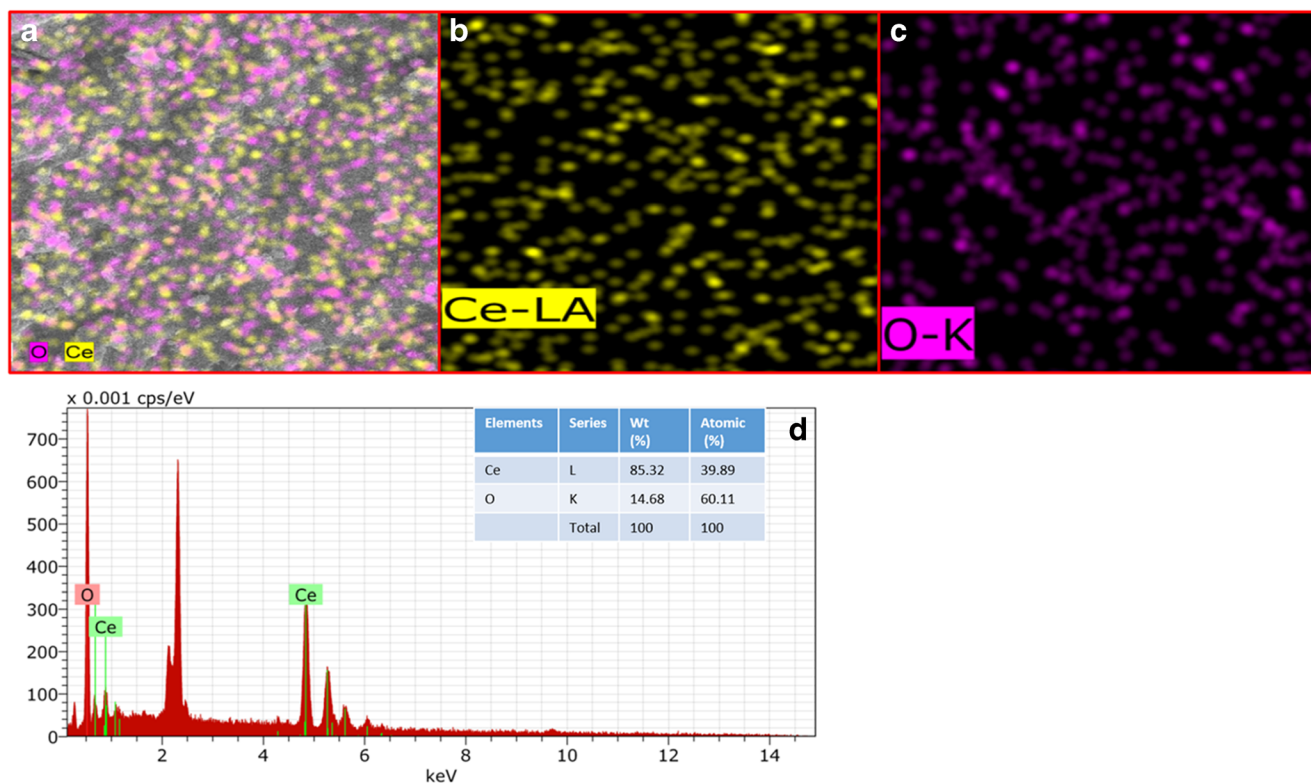
Fig. 4 EDX spectrum and map of synthesized CeO$_2$ QDs via SDS: **a** Cerium (Ce)—oxygen (O), yellow and pink in the panel. **b** Cerium (Ce)—yellow in the panel. **c** Oxygen (O)—pink in the panel. **d** 2D spectrum. Inset table shows different compositions of Ce and O
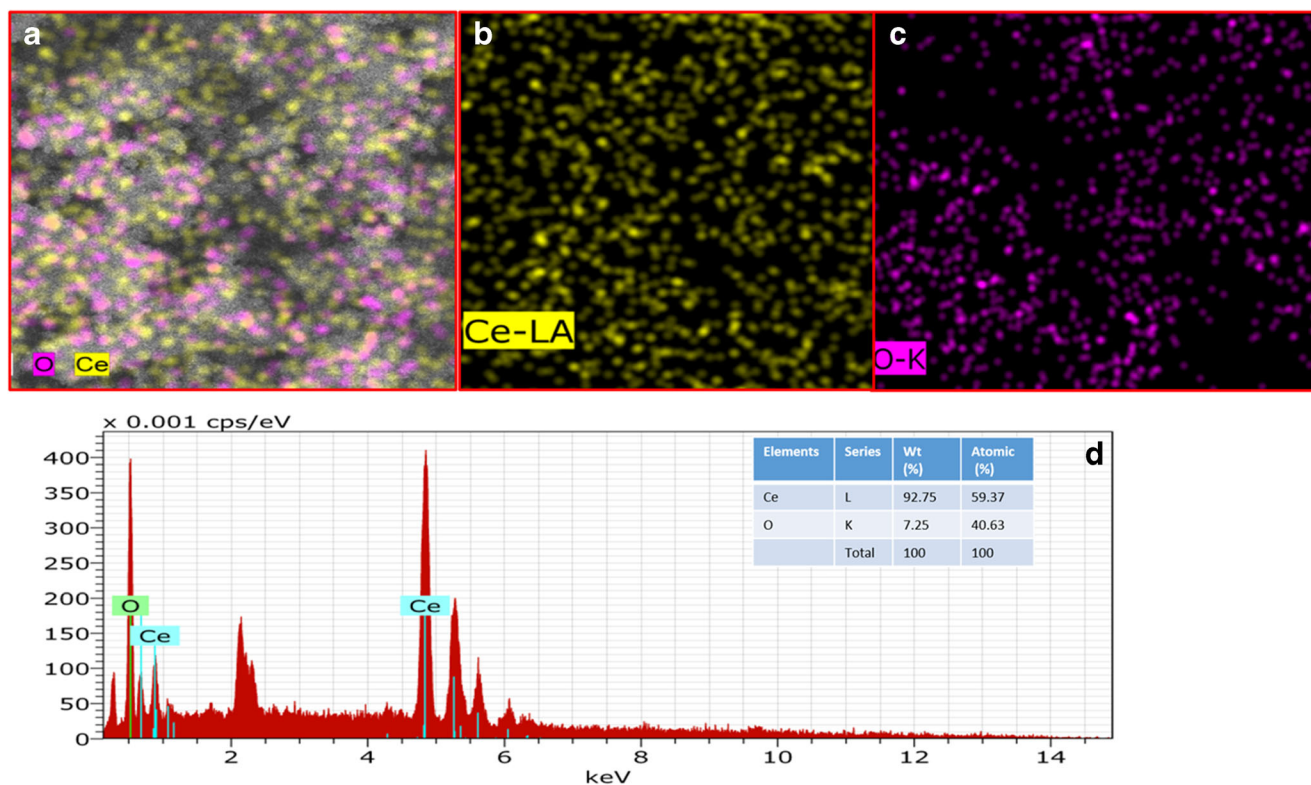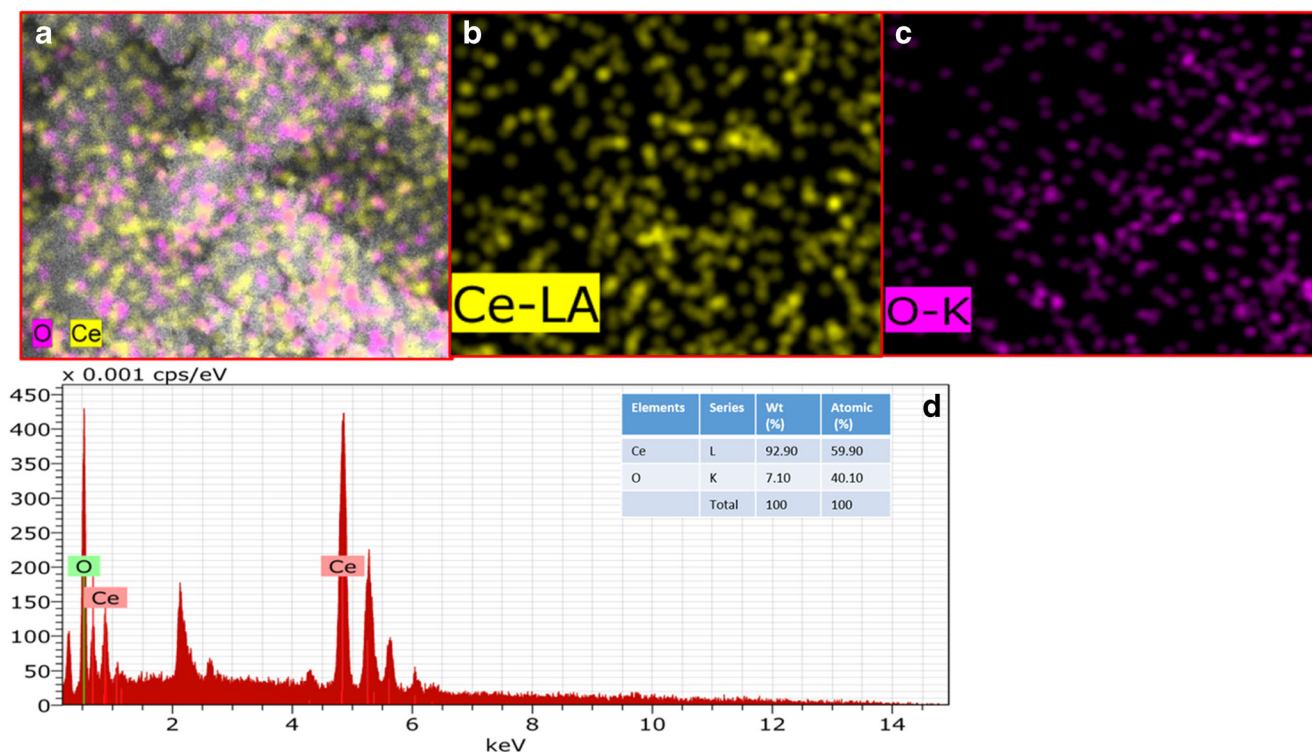

Fig. 5 EDX spectrum and map of synthesized CeO$_2$ QDs via CTAB: **a** Cerium (Ce)—oxygen (O), yellow and pink in the panel. **b** Cerium (Ce)—yellow in the panel. **c** Oxygen (O)—pink in the panel. **d** 2D spectrum

Fig. 6 EDX spectrum and map of synthesized CeO$_2$ QDs via CPC: **a** Cerium (Ce)—oxygen (O), yellow and pink in the panel. **b** Cerium (Ce)—yellow in the panel. **c** Oxygen (O)—pink in the panel. **d** 2D spectrum

with some spherical and elongated shapes of agglomerated particles. Particle size changes in changing the surfactants.

Energy-dispersive X-ray (EDX) microanalysis is a technique used for the identification of the elemental composition of a material. Figures 4, 5, and 6 show the composition of prepared CeO$_2$ nanoparticles, which all were examined by EDX. As proven by EDX, there were no other elements other than cerium and oxygen atoms. According to the EDX spectrum, prepared CeO$_2$ nanoparticles were pure and had no free surfactant or impurity. The optical analysis of the CeO$_2$ (SDS) QDs yielded 85.32% of Ce and 14.68% of O, CeO$_2$ (CTAB) QDs yielded 92.75% of Ce and 7.25% of O, and CeO$_2$ (CPC) QDs yielded 92.90% of Ce and 7.10% of O by weight (inset

table in Figs. 4d, 5d, 6d). Elemental mapping software determines the concentration of both elements Ce and O using two different colors, pink and yellow. The color is coded to indicate the relative concentration of both elements. Figures 4a, 5a, and 6a show the presence of both elements, while Figs. 4 b and c, 5 b and c, and 6 b and c give the individual mapping of cerium and oxygen.

HRTEM images give us appropriate information about morphology, size, and size distribution of the obtained particles. The surfactant addition enhanced both physical and/or chemical properties, for instance, surface area and particle size [15]. Figure 7 a–c illustrate the typical degree of agglomeration and the average particle sizes by HRTEM images of three
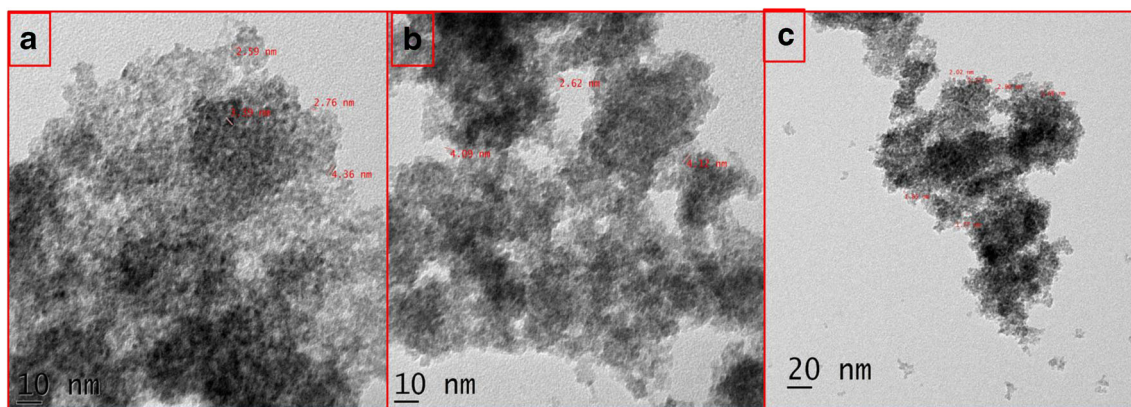

Fig. 7 HRTEM images of as-synthesized CeO$_2$ QDs: **a** SDS, **b** CTAB, and **c** CPC
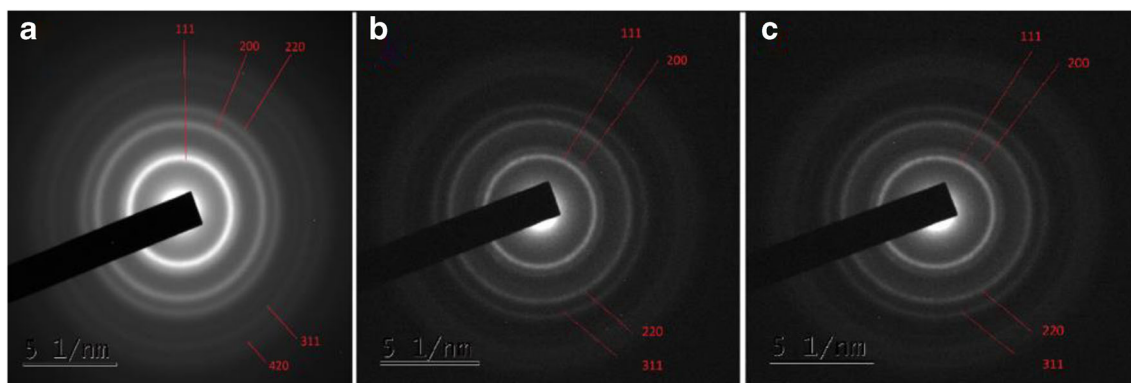
Fig. 8 SAED patterns of as-synthesized CeO_2 QDs: **a** SDS, **b** CTAB, and **c** CPC

different CeO_2 QDs by using three different surfactants (1.66–4.36 nm). Using HRTEM analysis, the analysis of the selected area electron diffraction patterns (SAED) of single quantum dots has been also performed. SAED patterns show the polycrystalline nature of CeO_2 QDs. A fringe array of spots corresponding to 111, 200, 220, and 311 planes (Fig. 8 a–c) shows the polycrystalline nature of obtained CeO_2 quite consistent with XRD results. Thus, it confirms its cubic phase structure.

The obtained sizes of these resulting nanoparticles in present investigation have been compared with previously reported data in literature (Table 2).

Moreover, Fig. 9 a–c show a thermogravimetric analysis (TGA) curves for CeO_2 prepared by different surfactants in the range of 10–800 °C. The TGA curves show the decomposition steps of CeO_2 with changing temperature. The order of CeO_2 stability by using different surfactants is CPC (86.29%) > CTAB (85.909) > SDS (77.9 %). For SDS- and CPC-synthesized CeO_2, there is a rapid loss in weight, from 200 to 450°C; rate of decomposition becomes slow, 450–500°C; again, rapid loss is noted, while after 500–800°C, weight loss becomes constant. While for CTAB-synthesized CeO_2, we found a continuous weight loss from 40 to 200°C.

After 200°C, weight loss becomes slow and after 400°C, it becomes constant. The weight loss is due to both losses of moisture and decomposition of hydrated oxide of cerium to cerium oxide. The remaining is due to the combustion of any organic residue. The weight loss of the sample is slowly inhibited beyond 600°C, which might be attributed to the pure CeO_2 phase formation.

In order to confirm the synthesis of the CeO_2 phase, Fourier transforms infrared (FTIR) spectra were recorded using KBr pellets, and the functional groups were identified.

Figure 10 shows the FTIR spectra of different surfactant-assisted CeO_2. These have several significant absorption peaks recorded in the 4000–400-cm^{-1} range. Broad absorption peaks at 3000–3913 cm^{-1} are assigned to OH stretching vibration of water in the sample, while the peaks at 1396 and 1541 cm^{-1} correspond to physically adsorbed water molecules. The band at 1082 cm^{-1} is due to atmospheric carbon dioxide since cerium oxide readily absorbs atmospheric water and air. FTIR spectra illustrated absorption peaks at 843 cm^{-1} and 660 cm^{-1}, which are the typical peaks of Ce-O stretching.

3.2 Kinetic study

For the kinetic study, the CeO_2 phase/nanomaterials synthesized via a CPC-mediated methodology were used because of smaller size particles. We also studied its degradation efficiency along with SDS- and CTAB-mediated synthesized CeO_2 and no major change in degradation at room temperature was marked. But close examination revealed that compared with SDS- or CTAB-synthesized CeO_2, CPC-mediated CeO_2 gave better results (Fig. 11a,). Thus, and for any overall degradation process, we used the CeO_2 synthesized via CPC.

The reaction was carried out with (A) only H_2O_2, (B) only CeO_2 QDs, and (C) both combined H_2O_2 and CeO_2 under sunlight. Either hydrogen peroxide or CeO_2 alone is insufficient to remove MB, while in the presence of both hydrogen peroxide and CeO_2 QDs, degradation/removal rate was significantly increased. H_2O_2 is a weak oxidizing agent and

Table 2 Particle size of CeO_2 NPs

S. no.	Characterization techniques	Particle size (nm)	References
1	SEM	142	[35]
2	TEM and XRD	20	[36]
3	SEM	100–300	[37]
4	SEM	23	[38]
5	TEM and XRD	10–20	[39]
6	SEM	160–180	[40]
7	SEM	30–66	[41]
8	SEM	15–30	[42]
9	HRTEM	11–21	[43]
10	HRTEM	1.66–4.36 nm	Present work

Fig. 9 TGA curves of CeO$_2$: **a** SDS, **b** CTAB, and **c** CPC
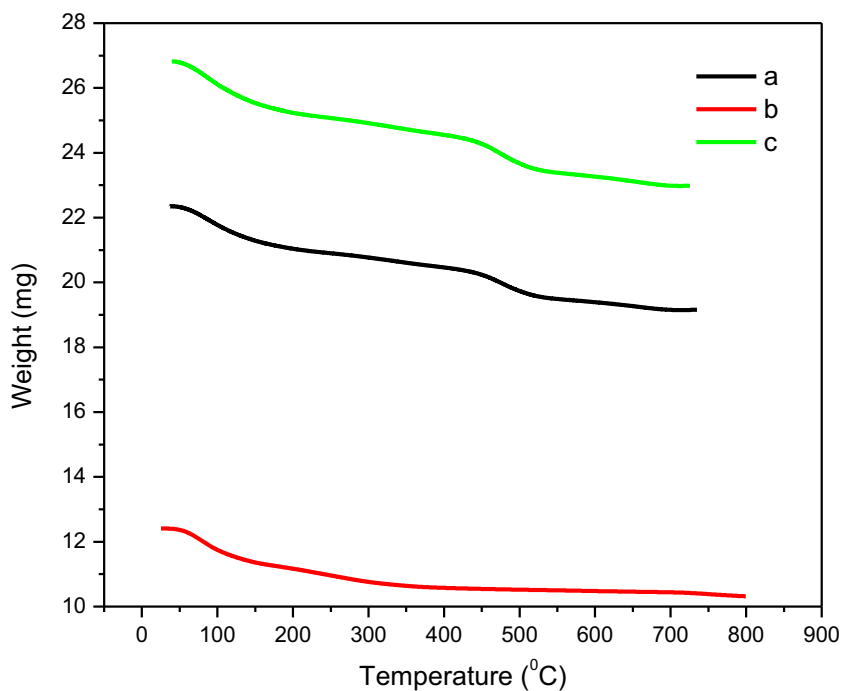
CeO$_2$ nanoparticles act as adsorbent when used alone. So, a combination of H$_2$O$_2$ and CeO$_2$ nanoparticles gave the best degradation result. The kinetic results can be understood by an interaction between hydroxyl radical and MB. 120 min was sufficient for complete removal of MB (Fig. 11b). Rate constant and percentage of removal are presented in Table 3.

Figure 11 c clearly shows the color removal of MB within 120 min under solar light. Removal efficiency can be calculated by the following equation:

$$\text{Removal effeciency} = C_0 + C\frac{}{C_t} \times 100 \tag{7}$$

where C_0 is the initial absorbance and C_t is absorbance after equilibrium. The efficacy of Fenton degradation is mainly based on the medium pH. From Fig. 12a, it is clear that maximum removal has occurred at pH 6 within 120 min. At lower pH (less than 6), excess of H$^+$ can act as a scavenger to reduce hydroxyl radicals to slow-down the removal efficiency. While

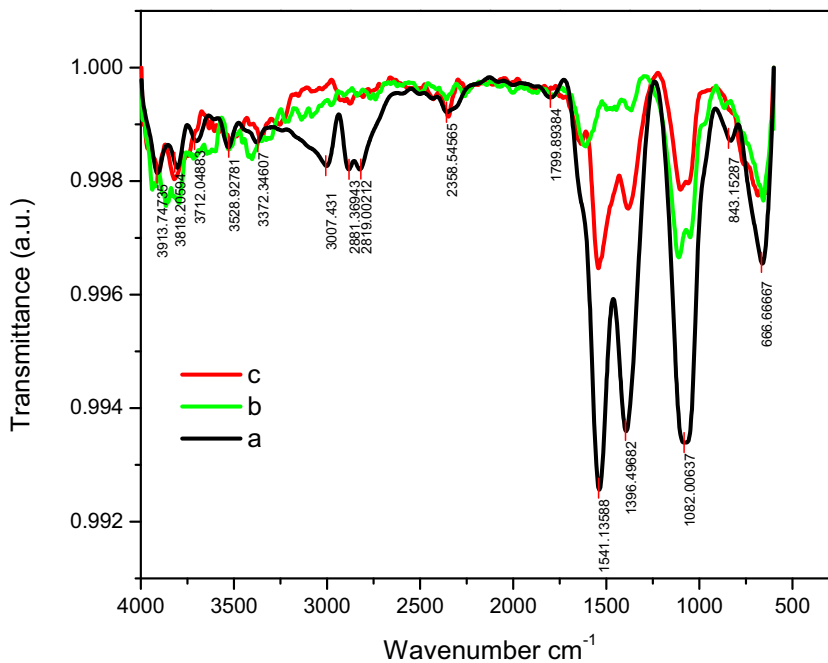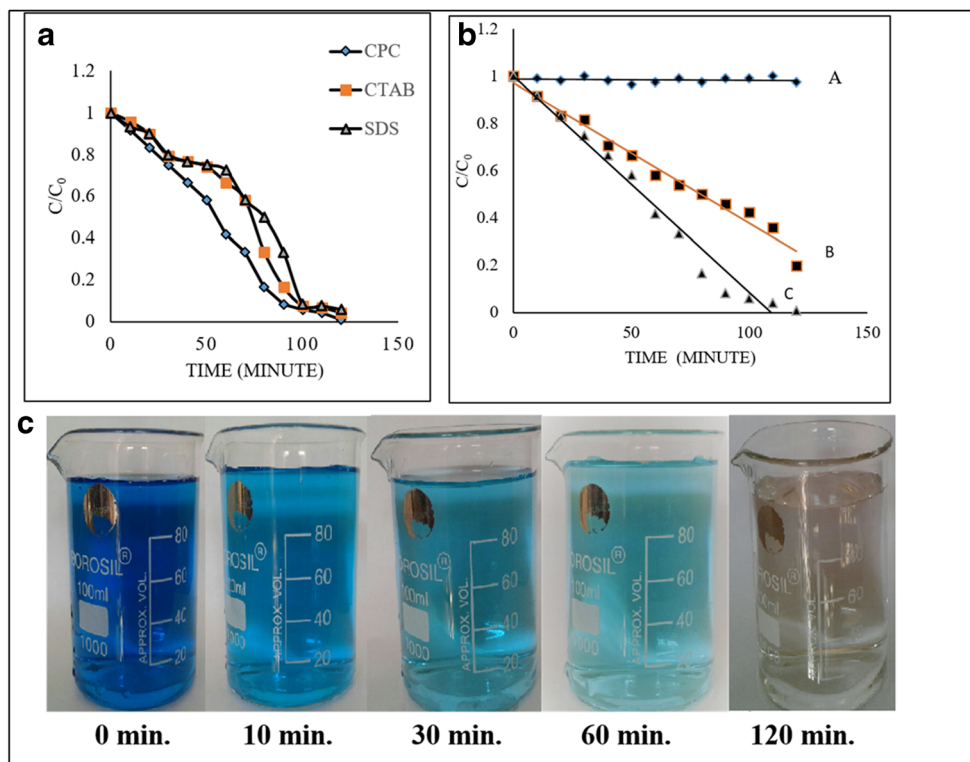**Fig. 10** FTIR spectra of CeO$_2$ QDs: **a** SDS, **b** CTAB, and **c** CPC

at higher pH (more than 6), H_2O_2 gets decomposed into water and molecular oxygen with less formation of hydroxyl radicals. Thus, assessment of the effect of pH was initially investigated and it was concluded that at pH 5–7, a higher degradation occurred.

Figure 12 b shows the effect of the addition of the catalyst, i.e., different doses of CeO_2 QDs (from 0.1 to 0.9 g/L) at constant concentrations of other variables at pH 6 to know its optimum catalytic efficiency. As the amount of CeO_2 QDs increases from 0.1 to 0.5 g/L, the degradation of MB has also increased, but after that, a little retardation effect is marked. As we know, the catalyst generates hydroxyl radicals from hydrogen peroxide for the removal/degradation process and access of active sites in catalyst retarded the degradation process. So, in the present case at initial concentrations, the catalyst easily generates hydroxyl radicals and may be at higher concentration acts as hydroxyl radical scavenger.

Studying the effects of variations of hydrogen peroxide has great importance because it is the only source to generate hydroxyl radicals for the radical degradation process. Figure 12 c depicts the degradation of MB at different concentrations of hydrogen peroxide (6 to 30 mmol/L) while keeping any other reaction conditions constant. Thus, it was observed that at initial concentrations (6 to 18 mmol/L) of oxidant, the degradation rate is increased while at higher concentrations, i.e., rate (24 to 30 mmol/L), it gets retarded. Since at higher concentrations, H_2O_2 autodecomposes and ultimately increases pollution and decreases the degradation rate.

From such results, it is concluded that the optimum concentrations of catalyst and H_2O_2 are 0.5 g/L and 18 mmol/L respectively for the degradation of 15 mg/L MB dye (pH 6) in the presence of sunlight.

These dissolved CeO_2 QDs are basically applied in small amounts and can be readily separated through centrifugation, firstly at 800 rpm for 2 min then 2000 rpm for 10 min. The catalytic activity was determined by its potential reusability for further reaction. In a recycling experiment, the CeO_2 QD catalyst was reused in five consecutive cycles for degradation of MB with little loss of activity of catalyst activity (Fig. 12d). In each cycle, the CeO_2 phase was isolated from the reaction set up at the end of the reaction, and then the separated particles were washed with ethanol and heated at 100 °C to remove extra impurities and moisture. There is only a quite low
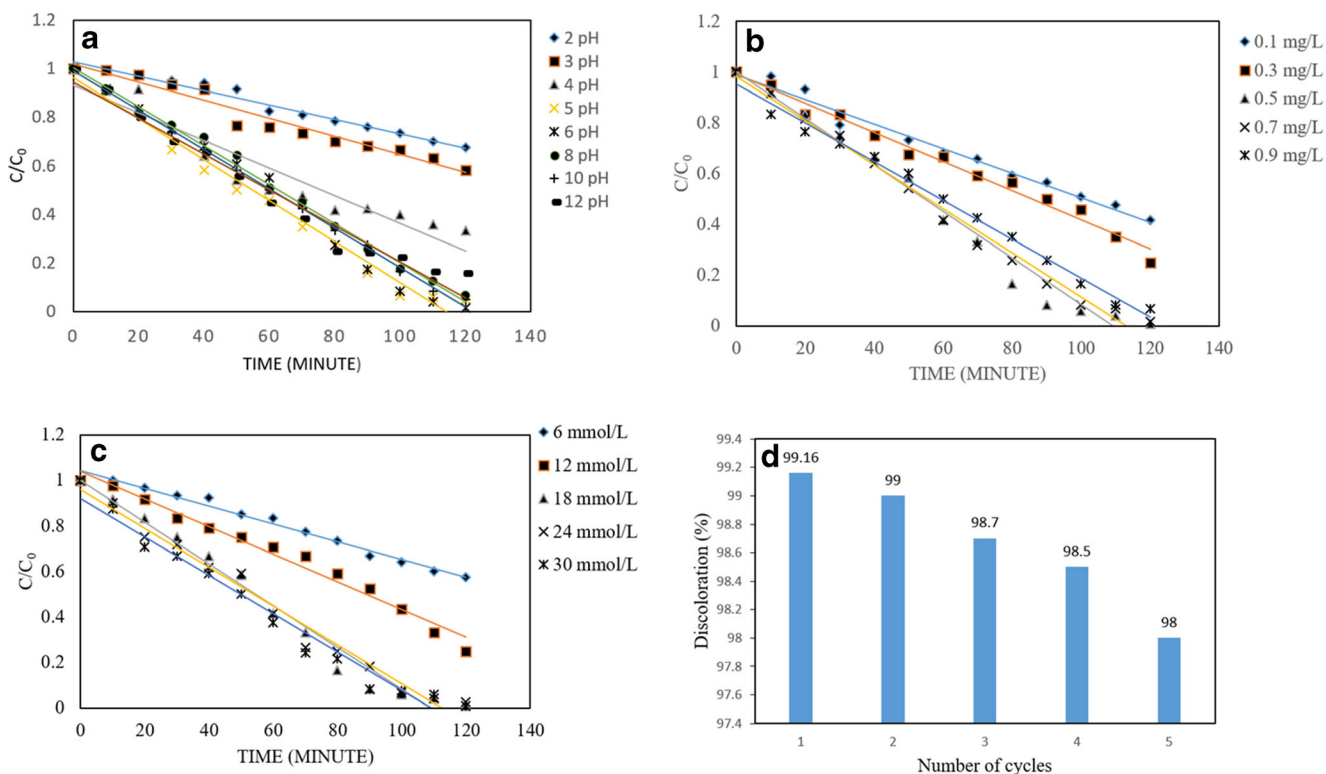
Table 3 Rate constant for degradation of MB in different conditions

S. no.	Reaction conditions	$k \times 10^4$ (min^{-1})	Removal (%)
1	MB + H_2O_2	1.92	2.50
2	MB + CeO_2	2.30	66.66
3	MB + H_2O_2 + CeO_2 + sun light	3.54	99.16

Fig. 12 MB removal: **a** effect of pH variation, **b** effect of catalyst dosage, **c** effect of [H_2O_2] dosage, **d** recycling test of CeO₂ QDs for MB degradation. Reaction conditions: H_2O_2 = 18 mmol/L, CeO₂ (CPC) = 0.5 g/L, MB = 15 mg/L, pH = 6 under sunlight

level of 2% loss of catalyst effectiveness obtained in 5 cycles. This low loss inactivity might be due to the continuous interconversion of Ce^{3+} to Ce^{4+}.

3.3 Mechanism of CeO₂ QD nanofabrication and MB degradation

In order to understand the effects of surfactant in the fabrication of CeO₂ particles, one can compare the present results with previously reported data [18, 19]. In this present work, the addition of surfactant decreases the size of obtained particles reaching a QD range (1–10 nm). Figure 13 shows a schematic diagram for the synthesis of CeO₂.

On the basis of our findings and literature, we proposed a plausible mechanism (Eqs. 8–15). Initially, unstable Ce^{3+} reacts with H_2O_2 in aqueous media to convert into Ce^{4+} with the generation of •OH. Then, such metallic Ce^{4+} cations further react to generate hydroperoxy radicals. Soluble Ce^{3+} and Ce^{4+} cations are easily interconverted to each other and easily oxidized by hydrogen peroxide to release hydroxyl radicals, which are more capable than hydrogen peroxide and hydroperoxy radicals to degrade MB.
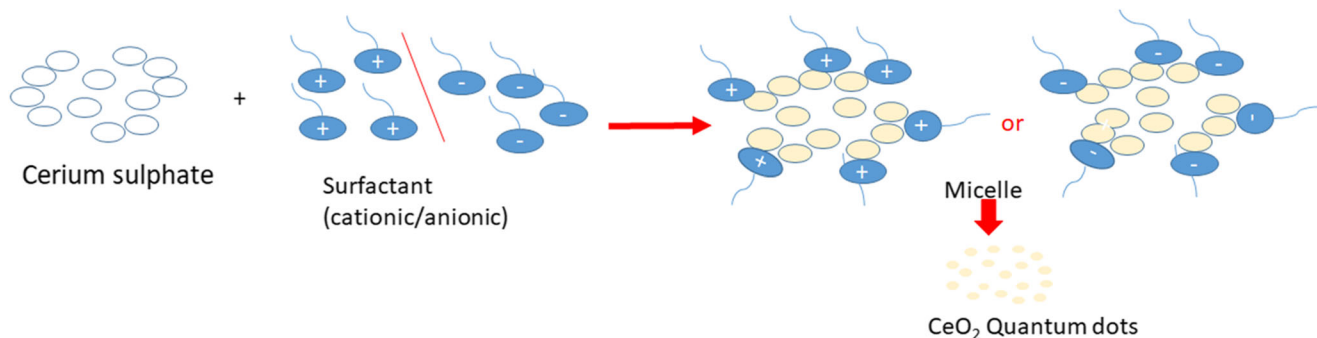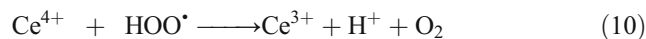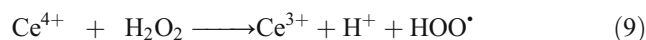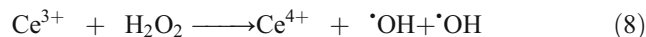
$$Ce^{3+} + H_2O_2 \longrightarrow Ce^{4+} + {}^{\bullet}OH + {}^{\bullet}OH \tag{8}$$

$$Ce^{4+} + H_2O_2 \longrightarrow Ce^{3+} + H^+ + HOO^{\bullet} \tag{9}$$

$$Ce^{4+} + HOO^{\bullet} \longrightarrow Ce^{3+} + H^+ + O_2 \tag{10}$$

Fig. 13 Proposed schematic diagram of cerium oxide synthesis

$$Ce^{3+} + {}^{\bullet}OH \longrightarrow Ce^{4+} + OH^{\bullet} \qquad (11)$$

$${}^{\bullet}OH + H_2O_2 \longrightarrow H_2O + HOO^{\bullet} \qquad (12)$$

$$Ce^{3+} + HOO^{\bullet} \longrightarrow Ce^{4+} + HOO^{-} \qquad (13)$$

$${}^{\bullet}OH + {}^{\bullet}OH \longrightarrow H_2O_2 \qquad (14)$$

$${}^{\bullet}OH + MB \longrightarrow Product + CO_2 + H_2O \qquad (15)$$
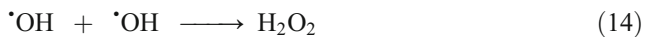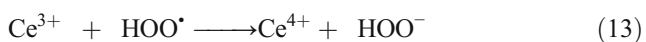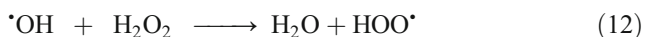
The experimental data strongly support the proposed mechanism for the degradation of MB in which nanofabricated CeO_2 QDs react with hydrogen peroxide to generate hydroxyl radicals, which subsequently attack/radically react to the MB species.

4 Conclusion

CeO_2 nanoparticles could be successfully synthesized by chemical precipitation method mediated by different cationic and anionic surfactants. CPC-mediated CeO_2 particles showed the smallest size as compared with the SDS- and CTAB-mediated ones. The particle size is less than 10 nm and thus is confined in a quantum range. CeO_2 QDs prepared via CPC served as catalyst species for heterogeneous Fenton reaction to successfully degrade MB at pH 6 under sunlight. About 99.16% discoloration of MB obtained was with hydrogen peroxide and CeO_2 under sunlight, while 66.66% removal occurred only with hydrogen peroxide and CeO_2 and less than 2.50% color removal could be achieved by degradation with only hydrogen peroxide. At the end of the degradation reaction, CeO_2 QDs could be successfully separated out from the reaction mixture by centrifugation and washed properly for the next combined use. This specific point/data output strongly confirms its stability and potential reuse.

Compliance with ethical standards

Conflict of interest The authors declare that they have no conflict of interest.

References

1. Girma WM, Fahmi MZ, Permadi A, Abate MA, Chang JY (2016) Synthetic strategies and biomedical applications of I-III-VI ternary quantum dots. J Mater Chem B 5:6193–6216

2. Chen D, Chen X (2019) Luminescent perovskite quantum dots: synthesis, microstructures, optical properties and applications. J Mater Chem C 7:1413–1446

3. Chen J, Patil S, Seal S, McGinnis JF (2006) Rare earth nanoparticles prevent retinal degeneration induced by intracellular peroxides. Nat Nanotechnol 1:142–150

4. Imanaka N, Masui T, Hirari H, Adachi G (2003) Amorphous cerium-titanium solid solution phosphate as a novel family of bandgap tunable sunscreen material. Chem Mater 15:2289–2291

5. Farias IAP, Santos CCLD, Sampaio FC (2018) Antimicrobial activity of cerium oxide nanoparticles on opportunistic microorganism: A systematic review. Biomed Res Int 2018: Article ID 1923606, p 14

6. Bamwenda GR, Arakawa HJ (2000) Cerium dioxide as a catalyst for water decomposition to O_2 in the presence of Ce_{aq}^{4+} and Fe_{aq}^{3+} species. J Mol Catal A Chem 161:105–113

7. Qian LW, Zhu J, Du WM, Qian XF (2009) Solvothermal synthesis, electrochemical and photocatalytic properties of monodispersed CeO_2 nanocubes. Mater Chem Phys 115:835–840

8. Zhai Y, Zhang S, Pang H (2007) Preparation, characterization and photocatalytic activity of CeO_2 nanocrystalline using ammonium bicarbonate as precipitant. Mater Lett 61:1863–1866

9. Das S, Dowding JM, Klump KE, McGinnis JF, Self W, Seal S (2013) Cerium oxide nanoparticles: application and prospects in nanomedicine. Nanomedicine 8(9):1483–1508

10. Vinothkannan M, Hariprasad R, Ramakrishnan S, Kim AR, Yoo DJ (2019) Potential bifunctional filler (CeO2-ACNTs) for nafion matrix toward extended electrochemical power density and durability in proton-exchange membrane fuel cells operating at reduced relative humidity. ACS Sustain Chem Eng 7:12847–12857

11. Gupta A, Das S, Neal CJ, Seal S (2016) Controlling the surface chemistry of cerium oxide nanoparticles for biological application. J Mater Chem B 4:3195–3202

12. Thill A, Zeyons O, Spalla O, Chauvat F, Rose J, Auffan M, Flank AM (2006) Cytotoxicity of CeO_2 nanoparticles for Escherichia coli. Physico-chemical insight of the cytotoxicity mechanism. Environ Sci Technol. 40:6151–6156

13. Lin WS, Huang YW, Zhou XD, Ma YF (2006) Toxicity of cerium oxide nanoparticles in human lung cancer cell. Int J Toxicol 25:451–457

14. Bumajdad A, Eastoe J, Mathew A (2009) Cerium oxide nanoparticles prepared in self assembled system. Adv Colloid Interf Sci 147-148:56–66

15. Terribile D, Trovarelli A, de Leitenburg C, Dolcetti G, Llorca J (1997) Unusual oxygen storage/redox behavior of high surface area ceria prepared by a surfactant assisted route. J Chem Mater 9:2676–2678

16. Terribile D, Trovarelli A, Llorca J, de Leitenburg C, Dolcetti G (1998) The synthesis and characterization of mesoporous high surface area ceria prepared using a hybrid organic/inorganic route. J Catal 178:299–308

17. Wu Z, Zhang J, Benfield RE, Ding Y, Grandjean D, Zhang Z, Ju X (2002) Structure and chemical transformation in cerium oxide nanoparticles coated by surfactant cetyltrimethylammonium bromide (CTAB): X-ray absorption spectroscopic study. J Phys Chem B 106:4569–4577

18. Kobayashi T, Iwamoto S, Inoue M (2006) Properties of the ceria particles prepared by solvothermal oxidation of cerium metal. J Alloys Compound 408-412:1149–1152

19. Sujana MG, Chattopadyay KK, Anand S (2008) Characterization and optical properties of nano ceria synthesized by surfactant mediated precipitation technique in mixed solvent system. Appl Surf Sci 254:7405–7409

20. Shang JT, Yang M, Zhang WL, Tan C, Han DJ (2012) Synthesis and characterization of nano cerium oxide by surfactant assisted precipitation method. Appl Mech Mater 286-270:180–183

21. Gnanam S, Rajendram V (2013) Influence of various surfactants on size, morphology, and optical properties of CeO₂ nanostructures via facile hydrothermal route, J. Nanoparticles 2013:1–6

22. Limbach LK, Bereiter R, Muller E, Krebs R, Galli R, Stark WJ (2008) Removal of oxide nanoparticles in a model wastewater treatment plant: influence of agglomeration and surfactants on clearing efficiency. Environ Sci Technol 42(15):5828–5833

23. Ramachandran M, Shanthi M, Subadevi R, Sivakumar M (2017) Role of surfactant on synthesis and characterization of cerium oxide (CeO₂) nanoparticles by modified co-precipitation method. Int Res J Eng Technol 4:31–35

24. Farahmandjou M, Zarinkamar M, Firozbadi TP (2016) Synthesis of cerium oxide (CeO₂) nanoparticles using simple co-precipitation method. Rev Mex Fis 62(5):496–499

25. Liu YH, Zuo JC, Ren XF, Yong L (2014) Synthesis and characterization of cerium oxide (CeO₂) nanoparticles by precipitation method. Metalurgija 53(4):463–465

26. Jayakumar G, Irudayaraj IA (2017) Particle size effect on the properties of cerium oxide (CeO₂) nanoparticles synthesized by hydrothermal method, A. D. Raj. Mech Mater Sci Eng J 9:127–131

27. Benmouhoub C, Kadri A, Benbrahim N, Hadji S (2009) Synthesis and characterization of cerium oxide (CeO₂) nanoparticles. Mater Sci Forum 609:189–194

28. Kumar E, Selvarajan P, Muthuraj D (2013) Synthesis and characterization of CeO₂ nanocrystals bysolvothermal route. Mater Res 16(2):269–276

29. Pol R, Ashwini K (2017) Cerium oxide nanoparticles: synthesis, characterization and study of antimicrobial activity. J Nanomater Mol Nanotechnol 6:3

30. Matei A, Tucureanu V, Tincu BC, Popescu M, Romanitan C, Cernica I, Dumitrescu LG (2017) Experimental aspects for CeO₂ nanoparticles synthesis and characterization. Metall Mater Sci 1:37–41

31. Tamizhdurai P, Sakthinathan S, Chen SM, Shanthi K, Sivasanker S, Sageetha P (2017) Environmentally friendly synthesis of CeO2 nanoparticles for the catalytic oxidation of benzyl alcohol to benzaldehyde and selective detection of nitrite. Sci Rep 7:46372

32. Sousa JCG, Ribeiro AR, Barbosa MO, Pereira MFR, Silva AMT (2018) A review on environmental monitoring of water organic pollutants identified by EU guidelines. J Hazard Mater 344:146–162

33. Huang C, Huang Y, Cheng H, Huang Y (2009) Kinetic study of an immobilized iron oxide for catalytic degradation of azo dye reactive black B with catalytic decomposition of hydrogen peroxide. Cataly Commun 10(5):561–566

34. Hsu CA, Wen TN, Su YC, Ziang ZB, Chen CW, Shyur LF (2012) Biological degradation of anthroquinone and azo dyes by a novel laccase from Lentinus sp. Environ Sci Technol 46(9):5109–5117

35. Piella J, Merkoci F, Zenc A, Arbiol J, Bastus NG, Puntes V (2017) Probing the surface reactivity of nanocrystals by the catalytic degradation of organic dyes: the effect of size, surface chemistry and composition. J Mater Chem A 5:11917–11929

36. Jafari N, Kasra-Kermanshashi R, Soud MR, Mahvi AH, Gharavi S (2012) Degradation of a textile reactive azo dye by a combine biological-photocatalytic process: Candida tropicalis jks2-TiO₂/UV. Iranian J Environ Health Sci Eng 9(33):1–7

37. Jain B, Singh AK, Sharma VK (2017) Degradation of napthylazo anionic dye by Fenton and Fenton like processes: a comparative study with Fast sulphon black-F. Desalin Water Treat 62:252–256

38. Pandit VK, Arbuj SS, Pandit YB, Naik SD, Rane SB, Mulik UP, Gosavic SW, Kale BB (2015) Solar light driven dye degradation using novel organo-inorgnic (6,13-pentacenequinone/TiO₂) nanocomposite. RSC Adv 5:10326–10331

39. Jain B, Singh AK, Sharma VK, Kim H, Lichtfouse E (2018) Treatment of organic pollutants by homogeneous and heterogeneous Fenton reaction processes. Environ Chem Lett 16:947–967

40. Duan X, Sun H, Shao Z, Wang S (2018) Nonradical reactions in environmental remediation processes: uncertainty and challenges. Appl Catal B Environ 224:973–982

41. Sinnat FS (1912) The use of methylene blue as an indicator in iodometric titration. Analyst 37:252–254

42. Vutskits L, Briner A, Klauser P, Gascon E, Dayer AG, Kiss JZ, Muller D, Licker MJ, Morel DR (2008) Adverse effect of methylene blue on nervous system. Anesthesiology 108:684–692

43. Dutta K, Mukhopadhyay S, Bhattacharjee S, Chaudhari B (2001) Chemical oxidation of MB using a Fenton like reaction. J Hazard Mater 84(1):57–71

44. Yang S, He H, Wu D, Chen D, Ma Y, Li X, Zhu J, Yuan P (2009) Degradation of MB by heterogeneous Fenton reaction using titanomagnetite at neutral pH values: process and affecting factors. Ind Eng Chem Res 48(22):9915–9921

45. Wang Q, Tian S, Ning P (2014) Degradation mechanism of MB in a heterogeneous Fenton like reaction catalyzed by ferrocene. Ind Eng Chem Res 53(2):643–649

46. Yang X, Chen W, Huang J, Zhou Y, Zhu Y, Li C (2015) Degradation of MB by heterogeneous Fenton reaction using titanomagnetite at neutral pH values: process and affecting factors. Sci Rep 5:10632

47. Vinothkannan M, Kartikeyan C, Kumar GG, Kim AR, Yoo DJ (2015) One pot green synthesis of reduced graphene oxide (RGO)/Fe3O4 nanocomposites and its catalytic activity toward methylene blue dye degradation. Spectrochim Acta A Mol Biomol Spectrosc 5:136

48. Yang S, He H, Wu D, Chen D, Liang X, Qin Z, Fan M, Zhu J, Yuan P (2009) Decolorization of MB by heterogeneous Fenton reaction using Fe₃₋ₓTiₓO₄ (0≤ x≤ 0.78) at neutral pH value. Appl Catal B Environ 89(3-4):527–535

49. Jain B, Hashmi A, Singh AK, Singh S, Susan MABH, Singh A (2020) Zinc oxide nanoparticle incorporated on graphene oxide: an efficient and stable photocatalyst for water treatment through the Fenton process. Adv Compos Hyb Mater. https://doi.org/10.1007/s42114-020-00153-5

50. Jain B, Hashmi A, Sanwaria S, Singh AK (2020) MABH Susan, SAC Carabineiro, Catalytic properties of graphene oxide synthesized by a "Green" process for efficient abatement of auramine-O cationic dye. Anal Lett 2:245–252